Electrically Enhanced Free Dendrite Growth in Polar and Non-polar Systems

K. G. Libbrecht[1], T. Crosby, and M. Swanson
Norman Bridge Laboratory of Physics, California Institute of Technology 264-33, Pasadena, CA 91125

[resubmitted to the Journal of Crystal Growth, November 5, 2001]

Abstract. We describe the diffusion-limited growth of dendritic needle crystals from the vapor phase, for which the application of an electrical potential to the crystal can profoundly affect the growth morphology, leading to an electrically induced morphological instability. With an improved theoretical treatment of this phenomenon, as well as new experimental data, we find the following below a threshold potential: 1) attachment kinetics is often more important than surface tension for selecting the Ivantsov solution in growth from the vapor phase, even in the absence of significant faceting; 2) the electrically modified growth velocity contains both polarization and electrostatic contributions, in contrast to previous treatments; 3) the threshold electrical potential is roughly independent of supersaturation, and 4) non-polar systems also exhibit the same electrically induced instability. Above threshold the underlying assumptions of solvability theory break down, and a new stabilization mechanism is required to explain the high-velocity shape-preserving needle growth observed in this regime. Guided by new electric needle data, we propose that the growth rates are being stabilized primarily by structural deformation driven by surface tension. We also describe the use of chemical additives to alter the needle growth axis and greatly increase the growth velocity.

1. Introduction

The formation of stable spatial patterns is a fundamental problem in the study of nonlinear non-equilibrium systems [1], and controlling pattern formation has generated considerable recent interest in light of a host of possible technological applications. A now-standard example of a condensed-matter pattern-forming system is the diffusion-limited growth of free crystalline dendrites, which are nearly ubiquitous products of rapid solidification, from either liquid or vapor precursors. While the diffusion equation alone is sufficient to define a relationship between the dendrite tip velocity and tip radius, typically anisotropic surface tension or attachment kinetics must be included in order to select a unique needle-like solution. Microscopic solvability theory has succeeded in furnishing a mathematically consistent and dynamically stable solution to this problem for simple 2D and 3D dendrite growth [2–4]. Instabilities and noise amplification leading to sidebranch generation have also been well studied [5].

Here we examine diffusion-limited shape-preserving needle growth from the vapor phase in the presence of an applied electrical potential. We previously described how high electric fields and

[1] Address correspondence to *kgl@caltech.edu*; URL: http://www.its.caltech.edu/~atomic/

field gradients near the needle tip can enhanced its growth, and subsequently drive in a new kind of instability in this system [6–9]. The growth behavior for small applied potentials is quite well described by an extension of normal dendrite growth theory, and we derive below an improved theoretical treatment of this phenomenon. This theory not only describes the behavior of the dendrite growth as a function of the applied potential, but it also explains the existence of the instability which occurs above a threshold potential.

The growth behavior above threshold is particularly interesting, and for some range of parameters we can still observe shape-preserving needle growth, albeit with much increased tip velocities. Above threshold the growth is still predominantly diffusion limited, so we retain the usual Ivantsov relation between the tip velocity and radius to a good approximation. However, the normal assumptions in solvability theory are no longer valid in this regime, and therefore the needle growth requires a new stabilization mechanism to select the correct Ivantsov solution. We performed a series of experiments to explore the physics of needle growth in this new electric regime, and from these we are able to examine the physical mechanisms responsible for selecting the enhanced needle growth rates.

Electrically modified dendrite growth is a useful tool for better understanding the general problem of pattern formation during solidification, in that it provides the experimenter with a new variable which affects the growth process. In addition, the phenomenon may also lead to interesting applications, such as the production of nanoscale metallic needle structures [10], processes for electrically mediated growth of nanotubes or polymers [11], and perhaps electrochemical modification of electrospin technologies [12].

2. Kinetics Limited Dendrite Growth from the Vapor Phase

Before examining electrically enhanced growth, it is instructive to first write down a theoretical treatment of normal diffusion-limited dendrite growth from the vapor phase in the presence of a solvent gas, focusing on a range of parameters appropriate for our experiments. While the underlying mathematics for normal growth from the vapor phase is essentially the same as for dendrite growth from the melt, there are two interesting differences: 1) the extreme density difference between the solid and vapor phases allows us to work in a very slow growth approximation, and 2) attachment kinetics is typically more important than surface tension in the selection problem, as we will see below. In this treatment we will ignore thermal effects arising from latent heat released during crystal growth, as this heat is fairly effectively carried away by the crystal and the solvent gas. This validity of this assumption is discussed quantitatively in the Appendix.

The timescale for diffusion to adjust the vapor concentration in the vicinity of a growing dendrite is $\tau_{diffusion} \approx R^2/D$, where R is the radius of the dendrite tip and D is the diffusion constant. This is to be compared with the growth time, $\tau_{growth} \approx R/v$, where v is the dendrite tip velocity. The ratio of these two timescales is given roughly by the Peclet number, $p = Rv/2D$. For our experiments growing ice dendrites in a solvent gas of air at a pressure of one atmosphere, we find $v \approx 5$ μm/sec, $R \approx 1$ μm, and $D = 2 \times 10^{-5}$ m^2/sec, so a typical value of the Peclet number is $p \approx 10^{-7}$. In this regime the diffusion length $\ell = 2D/v$ is of order 10 meters, much larger than the size of our

experimental apparatus. Thus the time-dependent diffusion equation for the particle concentration around the dendrite can be replaced by Laplace's equation, $\nabla^2 c = 0$, which must then be solved with the appropriate boundary conditions. The continuity equation at the interface yields

$$v_n = \frac{D}{c_{solid}} \left(\widehat{n} \cdot \overrightarrow{\nabla} c \right)_{surface} \tag{1}$$

for the normal growth velocity, where c_{solid} is the crystal density.

Our goal here is to describe the essential physics of dendrite growth in the presence of an applied potential, and not to find a mathematically precise solution to the full problem, so we will make some rather crude approximations when dealing with the dendrite geometry and the surface boundary conditions. This approach is instructive, quite productive, and is also an unfortunate necessity for several reasons: 1) the full problem of 3-D dendrite growth with significant attachment kinetics has not yet been solved (the 2D problem is described in detail in [3]); 2) the details of the attachment kinetics for ice growth from the vapor are not well known anyway; and 3) we will see that the exact problem becomes substantially more difficult when an electrical potential is introduced.

The contribution of surface energy to the surface boundary condition for a spherical crystal can be found by noting that the surface energy is $U_{surface} = 4\pi R^2 \gamma$, where γ is the surface tension, equal to 0.109 J m^{-2} for ice. Pulling a molecule off reduces the surface area and thus releases an energy

$$dU_{surface} = 8\pi R \gamma \frac{\partial R}{\partial N} = \frac{2\gamma}{c_{solid} R} \tag{2}$$

The contribution of this energy to the equilibrium vapor pressure goes like $e^{dU/kT}$, so to first order we have the equilibrium vapor pressure

$$c_{eq} \approx c_{sat} \left(1 + \frac{2d}{R} \right) \tag{3}$$

where $d = \gamma / c_{solid} kT$ and c_{sat} is the saturated vapor pressure above a flat interface.

Attachment kinetics in this case are obtained from the Hertz-Knudsen equation for growth from the vapor

$$\begin{aligned} v_n &= \alpha \sqrt{\frac{kT}{2\pi m}} \frac{(c_{surface} - c_{eq})}{c_{solid}} \\ &= \alpha v_{kin} \frac{(c_{surface} - c_{eq})}{c_{eq}} \end{aligned} \tag{4}$$

where $c_{surface}$ is the vapor concentration just above the surface and $\alpha \leq 1$ is the usual condensation coefficient. In the second expression we defined the characteristic kinetic velocity

$$v_{kin} = \frac{c_{eq}}{c_{solid}} \sqrt{\frac{kT}{2\pi m}} \tag{5}$$

which is a temperature-dependent quantity intrinsic to a given material. For our ice experiments $v_{kin} \approx 440$ μm/sec. Combining the Hertz-Knudsen equation with the above expression for c_{eq} then gives the boundary condition

$$c_{surface} \approx c_{sat} \left(1 + \frac{2d}{R} + \frac{v_n}{\alpha v_{kin}} \right) \tag{6}$$

This expression is strictly valid for spherical growth in the case of isotropic surface tension and attachment kinetics, but the general case will be similar in form.

We now assume that the crystal growth proceeds with a dendritic morphology, defined by an approximately parabolic dendrite tip moving at constant velocity. In our experiments the tip shapes

are only roughly parabolic, since the attachment kinetics are such that some faceting is observed. For many of our measurements, however, it appears that the dendrite tip is indeed rounded, perhaps the result of kinetic roughening, and the faceting becomes fully developed only along the body of the dendrite, where the growth is slower. We thus believe that the parabolic assumption is a reasonable one when describing our experiments. Here again our goal is not to solve the exact growth problem, but only describe the salient physical features of our experiments with electrically enhanced growth.

Diffusion-limited dendrite growth has been well characterized, and for the slow-growth limit from the vapor phase it is straightforward to show that the Ivantsov solution for growth of a 3D cylindrically symmetric parabolic crystal of tip radius R is [4, 7]

$$v \approx \frac{2D}{R \log(\eta_\infty / R)} \frac{c_{sat}}{c_{solid}} \left[\Delta_1 - \frac{2d}{R} - \frac{v}{\alpha v_{kin}} \right] \tag{7}$$

where $\Delta_1 = (c_\infty - c_{sat})/c_{sat}$ and η_∞ is the parabolic coordinate of the far-away boundary of the system, at which point we have $c = c_\infty$. This solution gives a relation between the tip velocity v and radius R, here with small perturbations from the capillary and kinetic terms (assuming $d \ll R$ and $v \ll \alpha v_{kin}$). The log term in this expression appears because we are in a regime where the diffusion length is larger than the boundaries of the experimental apparatus, *i.e.* $\ell \gg \eta_\infty$. In our case we estimate η_∞ / R is roughly between 10^4 and 10^5, which then gives $\log(\eta_\infty / R)$ between 9.2 and 11.5. Such small variations are negligible in our current treatment, so in what follows we will take $B \equiv \log(\eta_\infty / R) \approx 10$ to be constant. This is consistent with our expectation that the particular details of the far-away boundary condition in the problem – for example that the outer boundary is not in fact parabolic, so that η_∞ is not precisely defined – should not contribute greatly to the final solution.

When the growth is mainly diffusion limited we have $v \ll \alpha v_{kin}$, and we can substitute the unperturbed Ivantsov solution in for v on the right-hand-side of Eqn 7, which then gives to lowest order

$$v \approx \frac{2D}{BR} \frac{c_{sat}}{c_{solid}} \left[\Delta_1 - \frac{2d}{R} - \frac{R^*_{kin}}{R} \right] \tag{8}$$

where

$$R^*_{kin} = \frac{\Delta_1}{\alpha} \frac{2D}{B} \sqrt{\frac{2\pi m}{kT}} \tag{9}$$

$$= \frac{\Delta_1}{\alpha} R_{kin} \tag{10}$$

These results are analogous to the case of dendrite growth from a melt, in particular the treatment by Brener and Mel'nikov [3], where many aspects of the full solvability problem have been worked out in 2D when both capillary and kinetic boundary conditions are relevant. The length d defined above is essentially the same as the capillary length d in [3], and the length R^*_{kin} defined above is analogous to the length $pD\beta$ in [3] (*e.g.* see Eqn 9.2). (See also [14].) Note both lengths are assumed to be anisotropic with respect to the crystal axes.

In our ice experiments we have $d \approx 1$ nm and $R_{kin} \approx 30$ nm, and we expect the anisotropy in the attachment kinetics to be larger than the anisotropy in the surface tension. This is probably the case even when the growing crystal does not show significant faceting, since the anisotropy in d is only a few percent. Since in our experiments we have $\Delta_1 > 0.2$, it then stands to reason, given the results in [3], that the selection of the dendrite radius will be governed by attachment kinetics, and not by

surface tension. Furthermore we see that R_{kin} is linear in D but is not very strongly dependent on material properties. Thus we expect that attachment kinetics will often be more important than surface tension in the growth of dendrites from the vapor phase. For our subsequent analysis we will assume that capillary effects are negligible in comparison to attachment kinetics.

Following the analysis in [3], we then write down a dimensionless "solvability" parameter

$$\sigma_0 = \frac{2R_{kin}D}{vR^2}\frac{\Delta_1}{\alpha}\frac{c_{sat}}{c_{solid}} \tag{11}$$

which relates v and R, and we expect that σ_0 will be approximately independent of the extrinsic variables in the problem, and will depend only on the intrinsic material properties, particularly the degree of anisotropy in the attachment kinetics.

As has been noted in the context of solvability theory (*e.g.* [15]), Eqn 11 above follows mainly from the fact that attachment kinetics here provides the additional length scale R^*_{kin} necessary for uniquely determining the needle crystal shape. Calculating σ_0 from material properties, in particular the anisotropy of the attachment kinetics, would require a full 3D treatment of the dendrite problem including kinetics, which as yet does not exist. Instead we will simply assume that σ_0 is a constant to be determined from experiment, and proceed with the problem of calculating the additional effects of an applied electrical potential.

Note that combining the solvability parameter with the Ivantsov solution gives a tip radius that is independent of Δ_1,

$$R = \frac{B}{\alpha\sigma_0}R_{kin} \tag{12}$$

and a dendrite tip growth velocity

$$v = \frac{2D\alpha\sigma_0}{R_{kin}B^2}\frac{c_{sat}}{c_{solid}}\Delta_1 \tag{13}$$

which depends linearly on Δ_1, as is seen in the 2D solution [3].

3. Electrically Modified Dendrite Growth

When an electrical potential is applied to the growing crystal, the normal diffusion equation is replaced by the Smoluchowski equation [7, 13], which describes diffusion in the presence of an external force. In our case we have

$$\frac{\partial c}{\partial t} = D\overrightarrow{\nabla}\cdot(\overrightarrow{\nabla}c + c\overrightarrow{\nabla}\Phi) \tag{14}$$

where the external force felt by the solute molecules is described as the gradient of the effective potential

$$\Phi = -\frac{\xi}{kT}\left(\overrightarrow{E}\cdot\overrightarrow{E}\right) \tag{15}$$

where ξ is the molecular polarizability, and the electric field is the gradient of the electrical potential $\overrightarrow{E} = -\overrightarrow{\nabla}\varphi$ [7]. Again we will assume the slow-growth limit and take $\partial c/\partial t \approx 0$. The continuity equation at the interface yields the normal component of the surface growth rate as

$$v_n = \frac{D}{c_{solid}}\widehat{n}\cdot(\overrightarrow{\nabla}c + c\overrightarrow{\nabla}\Phi)|_{surf}. \tag{16}$$

The boundary condition at the crystal surface is now changed by the fact that the applied potential changes the equilibrium vapor pressure, which we can see most easily in the spherical case. Consider a spherical droplet of radius R and charge Q, where we assume the charge is localized at

the droplet surface. The electrostatic self-energy of this charge

$$U_{electrostatic} = \frac{1}{2}\frac{1}{4\pi\varepsilon_0}\frac{Q^2}{R} \tag{17}$$

is independent of the dielectric constant of the droplet, since there is zero field below the surface. If we pull one neutral molecule out of the droplet, then this changes $U_{electrostatic}$ by the amount

$$\begin{aligned} dU_{electrostatic} &= -\frac{1}{8\pi\varepsilon_0}\frac{Q^2}{R^2}\frac{\partial R}{\partial N} \\ &= -\frac{1}{32\pi^2\varepsilon_0}\frac{Q^2}{c_{solid}R^4} \end{aligned} \tag{18}$$

If the molecule has a nonzero polarizability, then pulling the molecule off the droplet releases the polarization energy

$$\begin{aligned} dU_{polar} &= \xi E^2 \\ &= \xi\frac{1}{16\pi^2\varepsilon_0^2}\frac{Q^2}{R^4} \end{aligned} \tag{19}$$

where $\xi \approx 3.4 \times 10^{-39}$ $\mathrm{C^2mN^{-1}}$ for a water molecule.

Again these energies contribute to the equilibrium vapor pressure like $e^{dU/kT}$, yielding for the spherical case (ignoring the surface energy contribution)

$$c_{surface} \approx c_{sat}\left(1 + \frac{v_n}{\alpha v_{kin}} - \frac{R_{es}^2}{R^2} + \frac{R_{pol}^2}{R^2}\right) \tag{20}$$

where $R_{es}^2 = \varepsilon_0\varphi_0^2/2c_{solid}kT$, $R_{pol}^2 = \xi\varphi_0^2/kT$, and $\varphi_0 = Q/4\pi\varepsilon_0 R$ is the electrical potential applied to the droplet. Note the presence of both electrostatic and polarization terms in this expression, the latter being zero for non-polar molecules. Throughout this discussion we will assume that the surface kinetics, parameterized by the condensation coefficient α, remains unchanged in the presence of the applied electrical potential. This is likely the case since the applied fields are too weak to significantly modify the surface molecular dynamics.

To derive the modified Ivantsov relation, first consider the spherical case, for which we have the growth velocity

$$v_n = \frac{D}{c_{solid}}\widehat{n}\cdot(\overrightarrow{\nabla}c + c\overrightarrow{\nabla}\Phi)|_{surf} \tag{21}$$

$$= \frac{Dc_{sat}}{Rc_{solid}}\left[\Delta_1 - \frac{R_{kin}^*}{R} + \frac{R_{es}^2}{R^2} - \frac{R_{pol}^2}{R^2} + \frac{1}{c_{sat}}\int_R^\infty c\,\frac{d\Phi}{dr}\,d\widehat{r}\right] \tag{22}$$

From the electrical potential of a charged droplet we have

$$\frac{d\Phi}{dr} = \frac{4\xi\varphi_0^2R^2}{kTr^5} \tag{23}$$

and for the concentration field we can approximate $c(r)$ in the integrand to be equal to the $\varphi_0 = 0$ solution

$$c_0(r) = c_\infty - \frac{R\triangle c}{r} \tag{24}$$

which then yields

$$v_n = \frac{Dc_{sat}}{Rc_{solid}}\left[\Delta_1 - \frac{R_{kin}^*}{R} + \frac{R_{es}^2}{R^2} + \frac{\Delta_1}{5}\frac{R_{pol}^2}{R^2}\right] \tag{25}$$

In the case of ice $R_{es} \approx 0.2(\varphi_0/1000\text{ V})$ μm and $R_{pol} \approx 1.0(\varphi_0/1000\text{ V})$ μm, so we see the electrostatic and electric polarization terms are of fairly comparable magnitude when $\Delta_1 \approx 0.2$; for higher values of Δ_1 the polarization term dominates.

The full parabolic case is clearly much more difficult to solve, and only an approximate treatment

has been demonstrated to date [7]. Following this we generalize the above and take the modified Ivantsov solution to be

$$v \approx \frac{2D}{BR}\frac{c_{sat}}{c_{solid}}\left[\Delta_1 - \frac{R^*_{kin}}{R} + C\frac{R^2_{elec}}{R^2}\right] \tag{26}$$

with

$$R^2_{elec} = \frac{2\varepsilon_0}{c_{solid}}\frac{\varphi_0^2}{B^2 kT} \tag{27}$$

where $C = 1 + 2\Gamma\xi c_{solid}\Delta_1/\varepsilon_0$ and $\Gamma \approx 0.2$.is a dimensionless geometrical constant. It is understood that this is only an approximate solution to the Smoluchowski equation, which takes the form of the normal Ivantsov solution (in the slow-growth limit) modified by several small additional terms. We expect that a full numerical solution would yield the same basic result, although probably with additional small geometrical corrections.

In the case of ice $R_{elec} \approx 40(\varphi_0/1000\text{ V})$ nm, and $2\xi c_{solid}/\varepsilon_0 = 23.5$, giving $C \approx 1 + 4.7\Delta_1$ at $T = -5$ C. The first analysis of this problem [6, 7] ignored the electrical perturbation of the equilibrium vapor pressure, an error which was pointed out by Brener and Muller-Krumbhaar [8] . We see here that the subsequent correction [8] was again incomplete, in effect assuming $\Gamma = 0$, which ignores the polarization term. For our present experiments this assumption is not a good one, since the polarization term is in fact larger than the electrostatic term. However since $C = 1$ when $\xi = 0$, we retain the theoretical prediction that an applied potential will also affect dendrite growth from non-polar molecules [8].

The electrical perturbation can be incorporated into the solvability relation by defining the modified length $R_{comb} \equiv R^*_{kin} - CR^2_{elec}/R$, and again assuming that this is the additional length scale necessary for uniquely determining the tip radius. This then yields the new solvability relation

$$\sigma_0 \approx \frac{2R^*_{kin}D}{vR^2}\frac{c_{sat}}{c_{solid}}\left(1 - C\frac{R^2_{elec}}{R^*_{kin}R}\right) \tag{28}$$

If the second term in the parentheses is $\ll 1$, we expect that σ_0 will again be roughly constant. Furthermore, taking $R_{elec} = 0$, we then see that the value of σ_0 must equal that obtained in the absence of an applied potential. Combining this with the modified Ivantsov relation then yields a quadratic equation for the tip radius [6]

$$R^2 - R_0 R + \frac{CR_0}{R^*_{kin}}R^2_{elec} = 0 \tag{29}$$

where R_0 is the tip radius when $R_{elec} = 0$.

The solution of the quadratic equation for small R_{elec} is

$$R \approx R_0\left(1 - \frac{C}{R^*_{kin}R_0}R^2_{elec}\right) \tag{30}$$

and

$$v \approx v_0\left(1 + \frac{C}{R^*_{kin}R_0}R^2_{elec}\right) \tag{31}$$

As R_{elec} increases, the tip radius decreases until a limit is reached when $R_{elec} = R_{elec,thresh} = (R^*_{kin}R_0/4C)^{1/2}$, at which point $R = R_{thresh} = R_0/2$ and $v = v_{thresh} \approx 2v_0$. Note $R^2_{elec,thresh}/R^2_{thresh} = R^*_{kin}/R_0C$ is always $\ll 1$ in our ice experiments, which supports the assumptions leading to Eqn 26. Since R_0 is independent of Δ_1, $R^*_{kin} \sim \Delta_1$, and $C \sim \Delta_1$ when dominated by polarization effects, so we expect $R_{elec,thresh}$ will be independent of Δ_1. Equivalently we expect that the applied electrical potential at threshold will be independent of Δ_1.

The quadratic equation above has no real roots when $R_{elec} > (R^*_{kin}R_0/4C)^{1/2}$, indicating that

the above modified solvability theory cannot be used for large R_{elec}, or equivalently when φ_0 is above some threshold potential φ_{thresh}. The lack of real roots indicates that above a threshold potential neither surface tension nor attachment kinetics can stabilize the tip radius, at least not in the usual sense of solvability theory. At this point the tip experiences runaway growth as $R \to 0$ under the influence of the Mullins-Sekerka instability (here enhanced by electric forces). The tip velocity thus increases until it is stabilized by some other mechanism, which we discuss further below.

Although the above treatment for electrically enhanced growth is very much incomplete, most of the theoretical uncertainty has been incorporated into the single parameter σ_0. Taking the next theoretical step, and predicting σ_0 from material parameters, appears to be an exceedingly difficult task. Furthermore, quantitative comparison of σ_0 with measurements would require a detailed knowledge of the anisotropy of the attachment kinetics, which would be itself difficult to attain. In spite of these problems, many aspects of electrically modified dendrite growth can be measured and compared with the results above.

4. Experiments with Dendrites Grown from Vapor

We performed a series of experiments using ice to observe normal and electrically modified dendrite growth from the vapor phase. Ice is a convenient material to work with in that it has a high vapor pressure, freezes at an easily accessible temperature, and it forms dendrites readily. Ice has also been very well studied, so many of its material properties are well characterized. Clearly dendrites grown from the vapor phase of other materials should exhibit a similar behavior, as dictated by theoretical considerations.

Electrical effects in the growth of ice crystals from the vapor was first described by Mason and collaborators [9], and we previously described additional details of the behavior of ice dendrites growth as a function of the applied electrical potential [6–8]. The existence of a threshold potential was established in these measurements, and the tip velocity as a function of φ_0 below threshold was found to be in good semi-quantitative agreement with the above theory. We have now extended these observations by measuring dendrite tip velocities as a function of supersaturation Δ_1 as well as φ_0, and have made many measurements above the threshold potential, where a different tip stabilization mechanism is required.

Our experiments were performed in air at atmospheric pressure, using a vertical diffusion chamber with a width and depth of 20 cm and a height of 30 cm. The bottom of the chamber was typically held at $T = -50$ C, and the supersaturation could be changed by adjusting the upper temperature, which was typically around $T = 40$ C [7]. Crystals were grown on the end of a thin wire placed inside the chamber from the bottom, to which an electrical potential could be applied. Supersaturation was determined using a combination of diffusion modeling and frost-point measurements, and we estimate an overall scaling uncertainty in our reported Δ_1 of roughly ± 30 percent.

Crystals grown at $T = -15$ C exhibited a classic dendritic morphology with growth along the a-axis, as is shown in Figure 1(a). These dendrites have an out-of-plane thickness of only some tens of microns (thicker far away from the growing tips), governed by strong faceting of the basal planes. It appears, however, that the faceting only becomes established some distance away from the tip,

and that the solid surface very near the tip is not faceted. The tip radius could not be resolved by our long-distance optical microscopy, and thus we could only place an upper limit of $R \lesssim 2$ μm from direct observations (see Figure 1). Tip velocities for these dendrites were observed to increase approximately linearly with Δ_1 as shown in Figure 2(a). At the lower supersaturation levels we observed stronger faceting of the prism planes near the dendrite tips, which corresponded to the deviation from the linear relationship at small Δ_1 seen in Figure 2(a).

Crystals grown at $T = -5$ C exhibited asymmetrical sidebranching, as is shown in Figure 1(b). At these high supersaturation levels the growth vector was typically displaced from the c-axis, as shown in Figure 1(b), with larger angular displacements toward the a-axis observed for larger Δ_1. Again it appeared that the region near the needle tip was not faceted, and again we could place an upper limit of $R \lesssim 2$ μm from direct observations. We measured tip velocities which increased linearly with Δ_1, as shown in Figure 2(b).

For our measurements at both $T = -5$ C and -15 C we see that the normal ($\varphi_0 = 0$) dendrite shapes were only roughly parabolic, so the Ivantsov solution is only an approximate one, and our analysis above can only be applied in an approximate sense. Nevertheless our data at both -5 C and -15 C clearly show tip growth which is approximately linearly dependent on Δ_1, as expected when kinetic effects predominate over the surface energy [3]. For the -15 C dendrites the points are roughly fit by $v = 5\Delta_1$ μm/sec, for which the Ivantsov solution yields $R_0 \approx 1.2$ μm independent of Δ_1 over this range. The relation

$$R_0 = \frac{B}{\alpha\sigma_0} R_{kin} \tag{32}$$

then gives $\alpha\sigma_0 \approx 0.25$. Similarly, the -5C data are reasonably well fit by $v = 9.5\Delta_1$ μm/sec, giving $R_0 \approx 1.5$ μm over this range of Δ_1, and $\alpha\sigma_0 \approx 0.2$.

Applying a small electrical potential (below threshold) to the growing crystals resulted in tip velocities that increased with increasing φ_0, and growth morphologies that were essentially unchanged from those at zero potential, as we reported earlier [6, 7]. In all cases we observed a well-defined threshold potential, beyond which the crystal growth was qualitatively different. We take this threshold potential to be the same as was calculated in the previous section. At $T = -15$ C we typically observed the tip-splitting phenomenon described in [7] when the potential reached its threshold value, so no tip velocities were made above threshold at this temperature. At $T = -5$ C we usually observed a fast-growing "electric needle" morphology above threshold, which exhibited no sidebranching and a constant tip velocity. Figure 3 shows an example of the electric needle morphology, for the case when the needle growth was along the c-axis of the ice crystal.

Figure 4 shows the tip velocities as a function of φ_0 at various Δ_1 for needle growth at -5 C, showing both the value of the threshold potential at each Δ_1 and the electric needle velocities above threshold. We observed a threshold potential of $\varphi_0 \approx 1000$ volts which was roughly independent of Δ_1, consistent with the above theoretical expectations. Our analysis then implies $R_{elec,thresh} \approx 40$ nm, and combining this with $R_0 = 1.5$ μm, and $C \approx 5.7$ (at $\Delta_1 = 1$) we find $R^*_{kin} = R_{kin}\Delta_1/\alpha = 24$ nm at $\Delta_1 = 1$, or $\alpha \approx 1$. A high value of the condensation coefficient is also suggested by the needle morphology, which shows little faceting near the needle tips. The more gradual velocity transition with increasing Δ_1 is not explained by our model.

Although the electric needles that grew above threshold were essentially featureless in their

morphology, the needle growth proceeded along different crystal axes, which could easily be discerned by removing the electrical potential and observing the subsequent normal growth, as demonstrated in Figure 3. In clean air at $T = -5$ C the needle growth was typically not along a principal crystal axis, like the growth of normal needles shown in Figure 1(b). It is the growth rates of these "clean air" electric needles that are plotted in Figure 4 and Figure 2(c).

Interestingly, we found that trace chemical additives in the air could have a dramatic effect on the electric needle growth, even when the concentration level was too low to produce any perceptible change in normal crystal growth. In particular, chemical additives could induce the electric needle growth to be along the ice c-axis, and such needles grew approximately four times faster than electric needles in clean air, as is shown in Figure 2(c). We found that a number of chemical additives at the 100 ppm level produced these rapidly growing needles, including various alcohols and acids, as well as chloroform, xylenes, methylene chloride, and even gasoline vapor. Acetic acid was particularly effective even at concentrations as low as 1 ppm, which produced essentially no change in the normal crystal growth. It appears likely that the additives are concentrated by the electric fields and gradients near the needle tip, thereby enhancing the chemical effects.

From the supersaturation dependence at $\varphi_0 = 2000$ volts (see Figure 2(c)) we infer tip radii of $R^* \approx 360$ nm for clean air electric needles using the Ivantsov relation, again independent of Δ_1. In the presence of chemical additives, the higher electric needle velocities imply $R^* \approx 90$ nm at $\varphi_0 = 2000$ volts, also roughly independent of Δ_1.

In a separate experiment, we examined the electric growth phenomenon for a non-polar molecular solid by examining the growth of iodine crystals from the vapor, again in a solvent gas of air at a pressure of one atmosphere [20]. At a supersaturation of $\Delta_1 \approx 0.1$ we obtained the results shown in Figure 5. Rapid needle growth above a threshold potential of $\varphi_0 \approx 1000$ volts was again clearly observed. The considerable scatter in the data above threshold may have resulted from competition between growing dendrites, although the scatter at $\varphi_0 = 0$ was much lower. These data provide qualitative support of the above theory, and clearly verify that this electrically induced morphological instability is present in non-polar systems.

5. Stabilization of Electric Needle Growth

When the applied electrical potential φ_0 is greater than the threshold value φ_{thresh}, the crystal growth at -5 C changes abruptly into the rapidly growing "electric needle" morphology described above. A notable feature of electric needles is that they exhibit shape-preserving growth with constant tip velocities, analogous to normal diffusion-limited dendrite growth. We see from the discussion above, however, that the theoretical machinery developed to describe normal dendrite growth can no longer be applied in the regime of electric needle growth, since at small tip radii the electric effects overwhelm the normal stabilization mechanisms. Thus we must address anew the question of what physical mechanism stabilizes the growth of electric needles, or equivalently what mechanism selects the correct Ivantsov solution.

The first step we can take in this direction is to rule out several possible candidate mechanisms. The latent heat generated by the condensing molecules appears to be inadequate for stabilizing the

tip growth, using the considerations in the Appendix. The calculated temperature increase is both small and roughly proportional to vR, and is therefore independent of the tip radius R to lowest order. Thus although tip heating will increase the saturation vapor pressure, and thus slow the needle growth slightly, it does not appear that this mechanism limits the electric needle growth. Further evidence for this statement comes from the growth data at 2000 volts, which show a linear dependence of growth velocity on Δ_1. Since tip heating increases with Δ_1, one would expect slower growth than is observed at the higher supersaturation levels.

Since we are applying a high voltage to the growing needle crystal, and the radius of curvature of the tip is as small as 90 nm, we must also consider field emission as an R-dependent source of tip heating that may stabilize the tip growth. From the Fowler-Nordheim relation [19]

$$I = A\frac{e^3}{8\pi hW}E^2 \exp\left[-\frac{8\pi 2^{1/2} m_e^{1/2}}{3he}\frac{W^{3/2}}{E}\right] \tag{33}$$

where A is the emission area, e is the electron charge, h is Planck's constant, W is the material work function, E is the surface electric field, and m_e is the electron mass. Using $W = 4.4$ eV $= 7.0 \times 10^{-19}$ J [17] and taking $A = R^2$ for the emission area, with $E = 2\varphi_0/\log(\eta_\infty/R)R$ for the parabolic case, this becomes

$$\begin{aligned} I &\approx \frac{e^3}{2\pi hW}\frac{\varphi_0^2}{\log(\eta_\infty/R)^2}\exp\left[-\frac{4\pi 2^{1/2} m_e^{1/2}}{3he}\frac{W^{3/2}\log(\eta_\infty/R)R}{\varphi_0}\right] \\ &\approx 0.014\text{A}\cdot\left(\frac{\varphi_0}{1000\text{ V}}\right)^2\cdot\exp\left[-312\left(\frac{R}{1\ \mu\text{m}}\right)\left(\frac{1000\text{ V}}{\varphi_0}\right)\right] \end{aligned} \tag{34}$$

where as above we have assumed $\log(\eta_\infty/R) = 10$. Assuming a power $P \sim I\varphi_0$ is deposited at the needle tip (likely an overestimate), and assuming the same simple thermal conduction model used in the Appendix, we estimate that tip heating becomes significant for $I \gtrsim 10^{-11}$ A. Ice conductance is high enough [17] that such low currents produce a negligible voltage drop along a needle, supporting our assumption of a constant electrical potential along the needle.

We measured the current emitted from growing needle crystals, and found there was a considerable dependence on the sign of the applied potential. For $\varphi_0 = 2000$ volts we found $I < 1$ pA under most circumstances and $I \approx 1$ pA for chemically mediated growth (with considerable scatter in the latter measurements). For $\varphi_0 = -2000$ volts we measured $I \approx 1 - 3$ pA without additives and $I \approx 10$ pA with additives (again with considerable scatter). These values are consistent with the Fowler-Nordheim relation, given the uncertainty in the various parameters. When $I \gtrsim 10$ pA we observed that the needle growth slowed substantially, and the tip velocities became quite variable from needle to needle.

We conclude from these results that field emission plays a significant role in our experiments with electric needle growth when $\varphi_0 = -2000$ and the crystals are grown in the presence of chemical additives, which results in sizable currents. In all other regimes it appears field emission does not limit the needle growth. Without chemical additives, or when the measured currents were below 1 pA, the needle growth rates were observed to be the same (to ± 15 percent) for positive and negative applied potentials.

Having eliminated thermal and field emission mechanisms, we propose that the diffusion-limited electric needle growth is stabilized by the diminished structural integrity of the material when formed into an extremely sharp tip. That is, the needle tip radius becomes so small that its solid structure

is subject to deformation driven by surface tension over timescales comparable to the crystal growth time $\sim R/v$. There is considerable uncertainty in our understanding of the structural properties of ice, particularly for such extremely small crystals, which makes detailed calculations difficult [17] . Surface melting certainly sets a lower bound on tip radius, since surface melting is known to produce a quasiliquid layer at these temperatures, which likely has very little resistance to shear stresses. The ice quasiliquid layer has a thickness of roughly 20 nm at $T = -5$ C [18], which is not insignificant compared to the tip radii inferred from our measurements.

Although this model is both speculative and difficult to quantify, it does explain the fact that in our measurements the tip radius R^* is essentially independent of Δ_1 and φ_0 in the electric growth regime (at least above a Δ_1-dependent transition region; see Figure 4). Above the threshold potential the tip radius decreases to the point that structural deformations become an important influence. This must occur at some material-determined size scale, so we would expect that the new tip radius would depend mainly on material properties, and would not depend strongly on supersaturation or the applied potential, as is observed. The change in R^* in the presence of additives could be explained by the strongly anisotropic structural properties of ice, since the most rapid growth observed is for c-axis needles, or by chemically induced changes in surface tension.

6. Discussion

In summary, we have examined the detailed physics of electrically enhanced diffusion-limited dendritic needle crystal growth from the vapor phase. When an applied potential is below a threshold value, we are able to adequately reproduce the measured needle growth velocity $v(\Delta_1, \varphi_0)$ using an electrical extension of solvability theory. One interesting feature of this theory, which is confirmed by our experiments, is that the needle tip selection is governed by attachment kinetics in this regime. Furthermore we expect that attachment kinetics will often be more important than surface tension in the diffusion-limited growth of dendrites from the vapor phase, as long as the supersaturation is fairly high.

Theory and experiment also reveal the existence of a threshold potential, beyond which the needle growth exhibits a morphological instability. Furthermore we see that the threshold potential φ_{thresh} is roughly independent of Δ_1 for highly polar molecules. Finally, we experimentally confirmed the theoretical prediction [8] that an applied potential will affect dendrite growth from non-polar molecules, which likewise exhibit a morphological instability above some φ_{thresh}.

We also examined in some detail the very interesting case of electric needle growth when $\varphi_0 > \varphi_{thresh}$, as this is a new physical regime in which the normal assumptions of solvability theory are not valid, and a new mechanism is required to stabilize the growth. Our measurements with ice suggest that electric needle growth in this system is usually not limited by the effects of latent heat deposition or field emission, and we propose that structural deformation of the needle tip is the likely stabilization mechanism.

Additional experiments with other materials would further elucidate the phenomenon of electric needle growth. In particular, since ice is a relatively soft material [17], these investigations suggest that harder materials could yield much sharper tips. Related experiments with refractory metals

have produced electric needle crystals with nanometer-scale tips [10]. We believe that additional research into electrically enhanced growth could potentially lead to useful applications.

7. Appendix – Consideration of Thermal Effects

Diffusion-limited dendritic growth from the vapor phase is a double diffusion problem, since in principle we must consider both particle diffusion to the growing crystal and thermal diffusion to remove the heat generated by condensation at the solid/vapor interface. In considering this joint diffusion problem it is useful to first examine the spherical case, which can be easily solved exactly in the slow-growth limit. Beginning with Laplace's equation for both the particle concentration field $c(r)$ and the temperature distribution $T(r)$, we find a growth velocity

$$v = \frac{D}{c_{solid}} \frac{\triangle c}{R} \tag{35}$$

which in turn produces a temperature increase

$$\triangle T = \frac{vR\lambda\rho}{\kappa_{solvent}} \tag{36}$$

Here $\triangle c = c_\infty - c_{surface}$ and $\triangle T = T_{surface} - T_\infty$, λ is the latent heat of condensation per unit mass, ρ is the solid mass density, and $\kappa_{solvent}$ is the thermal conductivity of the surrounding medium. Combining these yields the growth rate

$$v = \frac{D}{R} \frac{c_{sat}}{c_{solid}} \frac{\Delta_1}{1+\chi_0} \tag{37}$$

with $\Delta_1 = (c_\infty - c_{sat})/c_{sat}$, where c_{sat} is evaluated at T_∞, and

$$\chi_0 = \frac{d\ln(c_{sat})}{dT} \frac{D\lambda\rho}{\kappa_{solvent}} \frac{c_{sat}}{c_{solid}} \tag{38}$$

is a parameter which depends only on material properties and the diffusion constant. In the case of our ice experiments, $(1/c_{sat})(dc_{sat}/dT) \approx 0.1$ K^{-1}, $D = 2 \times 10^{-5}$ m^2/sec, $\lambda = 2.8 \times 10^6$ J/kg, $\kappa_{solvent} = \kappa_{air} \approx 0.025$ W m^{-1} K^{-1}, $\rho = 917$ kg/m^3 and $c_{sat}/c_{solid} \approx 10^{-6}$, giving $\chi_0 \approx 0.2$ at $T = -5$ C. We see the main effect of thermal transport is an effective rescaling of Δ_1 by about 20 percent.

The full parabolic case is of course much more difficult to solve, but a full solution is not necessary to examine the essential thermal effects. A crude but adequate model is to assume the dendrite growth to be a semi-infinite rod with radius equal to the dendrite tip radius R, with heat being deposited on the end of the rod [7]. The rate at which latent heat is deposited roughly is $\dot{Q}_{input} \approx \lambda\pi R^2 v\rho$, where v is the dendrite tip velocity, and heat conduction along the rod carries heat away from the end at a rate $\dot{Q}_{rod} \approx K_1 \kappa_{solid}(\pi R^2)\triangle T/L$, where $\triangle T = T_{tip} - T_{amb}$ is the temperature difference between the end of the rod and the ambient medium, K_1 is a dimensionless geometrical factor of order unity, and L is the effective distance from the end of the rod where the rod temperature approaches the ambient temperature. We expect $K_1 > 1$ for the parabolic case, since the conduction down a parabolic needle would be greater than for a straight rod. Finally, heat conduction into the ambient medium can be solved for the case of an infinite cylindrical rod, which gives $\dot{Q}_{air} \approx \kappa_{solvent} L \triangle T$.

In steady state we must have $\dot{Q}_{input} \approx \dot{Q}_{rod} \approx \dot{Q}_{solvent}$, which gives $L \approx K_1 \pi \left(\kappa_{solid}/\kappa_{solvent}\right)^{1/2} R$,

and we note that since $\kappa_{solid} \gg \kappa_{solvent}$ we have $L \gg R$. This then gives

$$\triangle T \approx \frac{1}{K_1} \frac{vR\lambda\rho}{\sqrt{\kappa_{solid}\kappa_{solvent}}} \tag{39}$$

analogous to Eqn 36. Combining this with the Ivantsov relation for vR gives a modified Ivantsov relation

$$v \approx \frac{2D}{BR} \frac{c_{sat}}{c_{solid}} \frac{\Delta_1}{1+\chi} \tag{40}$$

where here

$$\chi = \frac{2}{BK_1} \frac{d\ln(c_{sat})}{dT} \frac{D\lambda\rho}{\sqrt{\kappa_{solid}\kappa_{solvent}}} \frac{c_{sat}}{c_{solid}} \tag{41}$$

For the case of our ice experiments we have $\kappa_{solid} \approx 2.4$ W m^{-1} K^{-1} and we estimate $\chi \lesssim 10^{-3}$.

We can conclude from this analysis that for our experiments the thermal perturbation to the Ivantsov solution is very small, meaning that the dendrite growth is being limited primarily by particle diffusion, and not by thermal diffusion. Including the perturbations from surface tension and attachment kinetics yields

$$v \approx \frac{2D}{BR} \frac{c_{sat}}{c_{solid}} \left[\frac{\Delta_1}{1+\chi} - \frac{2d}{R} - \frac{v}{\alpha v_{kin}} \right] \tag{42}$$

in place of Eqn 7. Since χ is both very small and independent of R, we expect that thermal effects also contribute very little to the selection of the dendrite velocity, as would be dictated by a full solvability theory. We note, however, that d/R and v/v_{kin} are also fairly small, and our thermal analysis is quite crude. Thus it is conceivable that for our experimental parameters thermal effects do play some role in the selection problem, although we believe it is a negligible one.

8. References

[1] For reviews see E. Ben-Jacob, *Cont. Phys.* **38**, 205 (1997); *Cont. Phys.* **34**, 247 (1993); J. S. Langer, in *Chance and Matter: Les Houches Session XLVI* (Elsevier: New York, 1987); H. Muller-Krumbhaar, in *Materials Science and Technology: a Comprehensive Treatment* (R. W. Cahn *et al.*, eds) (VCH: Weinheim, 1991); M. C. Cross and P. C. Hohenberg, *Rev. Mod. Phys.* **65**, 851 (1993).

[2] E. Brener, *Phys. Rev. Lett.* **71**, 3653 (1993); A. Karma and W. J. Rappel, *Phys Rev. Lett.* **77**, 4050 (1996).

[3] E. A. Brener and V. I. Mel'nikov, *Adv. Phys.* **40**, 53 (1991).

[4] Y. Saito, *Statistical Physics of Crystal Growth* (World Scientific: Singapore) (1996), and references therein.

[5] E.Brener, D. Temkin, *Phys. Rev. E* **51**, 351 (1995).

[6] K. G. Libbrecht and V. M. Tanusheva, *Phys. Rev. Lett.* **81**, 176 (1998).

[7] K. G. Libbrecht and V. M. Tanusheva, *Phys. Rev. E* **59**, 3253 (1999).

[8] E. A. Brener and H. Muller-Krumbhaar, *Phys. Rev. Lett.* **83**, 1698 (1999); K. G. Libbrecht and V. M. Tanusheva, *Phys. Rev. Lett.* **83**, 1699 (1999).

[9] J. T. Bartlett, A. P. van den Heuval, and B. J. Mason, *Z. angew. Math. Phys.* **14**, 599-610

(1963).

[10] F. Okuyama, *Jpn. J. Appl. Phys.* **22**, 245 (1983); F. Okuyama, *Appl. Phys. A* **27,** 57 (1982).

[11] D. T. Colbert and R. E. Smalley, Carbon 33, 921 (1995).

[12] Y. M. Shin, M. M. Hohman, M. P. Brenner, G. C. Rutledge, *Appl. Phys. Lett.* **78**, 1149 (2001).

[13] S. Chandrasekhar, *Rev. Mod. Phys.* **15**, 1 (1943).

[14] A. A. Chernov, *Modern Crystallography III*, Springer Ser. Sol. St. Vol. 36, (Springer-Verlag) (1984).

[15] D. A. Kessler, J. Koplik, and H. Levine, *Adv. Phys.* **37**, 255 (1988).

[16] W. W. Mullins and R. F. Sekerka, *J. Appl. Phys.* **34**, 323 (1963); J. S. Langer, *Rev. Mod. Phys.* **52**, 1 (1980).

[17] V. F. Pentrenko and R. W. Whitworth, *Physics of Ice* (Oxford University Press: Oxford) (1999).

[18] Based on glancing incidence X-ray diffraction, H. Dosch, A. Leid, and J. H. Bilgram, *Surf. Sci.* **327**, 145 (1995); other observational techniques indicate substantially different quasiliquid layer thicknesses [17].

[19] R. H. Fowler, and L. Nordheim, Proc. R. Soc. London Ser. A, 119, 173 (1928); this specific form came from http://email.opt-sci.arizona.edu/summaries/Todd_Ruskell/fnpaper/fn11.htm.

[20] M. Swanson, *Caltech Undergraduate Research Journal* **1**, 48 (2001).

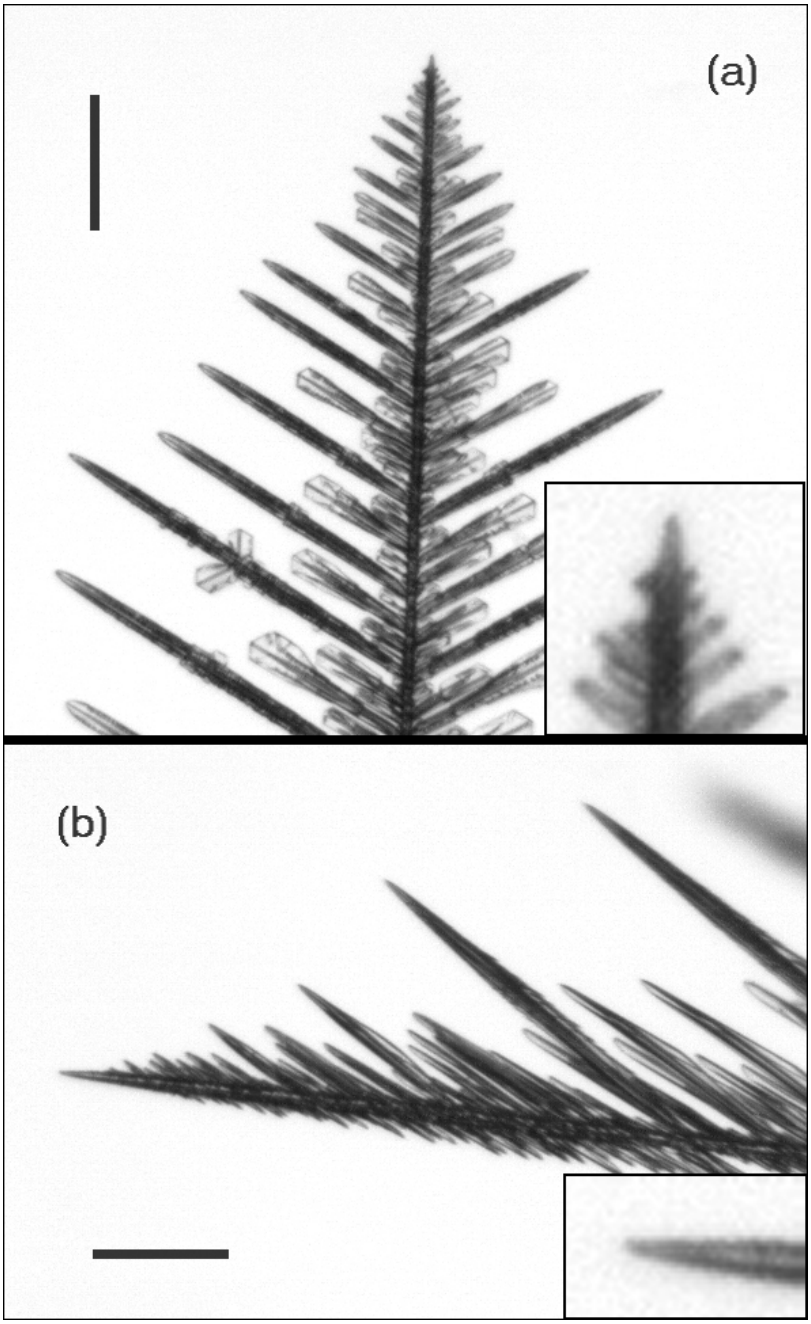

Figure 1. (a) Typical ice crystal dendrite grown at -15 C, which grows along the crystal a-axis and exhibits quasi-symmetrical sidebranching. (b) Typical -5 C ice crystal dendrite, showing asymmetrical sidebranching. Here the sidebranches are aligned roughly along the c-axis. Scale bars are 200 microns long for both figures. Insets show regions near the growing tips expanded 4x.

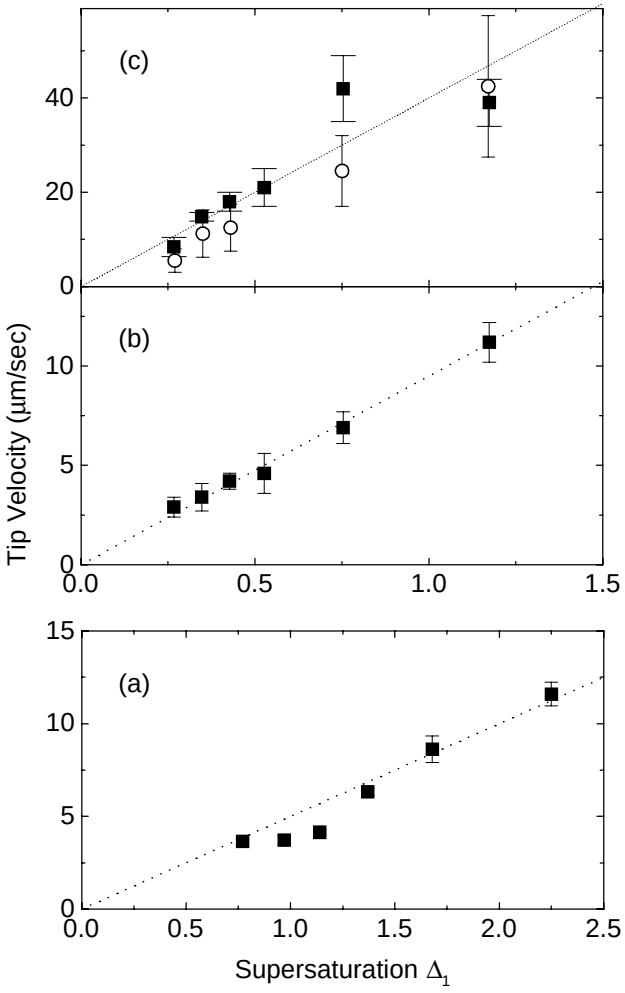

Figure 2. Tip velocities of growing ice needles, as a function of vapor supersaturation. (a) Dendrites grown at $T = -15$ C, with no applied potential; (b) Needle-like crystals grown at $T = -5$ C, again with no applied potential; (c) solid squares: v_{tip} for electric needles grown at $T = -5$ C with an applied potenial of 2000 volts; open circles: $v_{tip}/4$, for needles grown at $T = -5$ C and 2000 volts, but in the presence of vaporous chemical additives. These additives were used to promote growth along the c-axis, thus resulting in much faster growing needles.

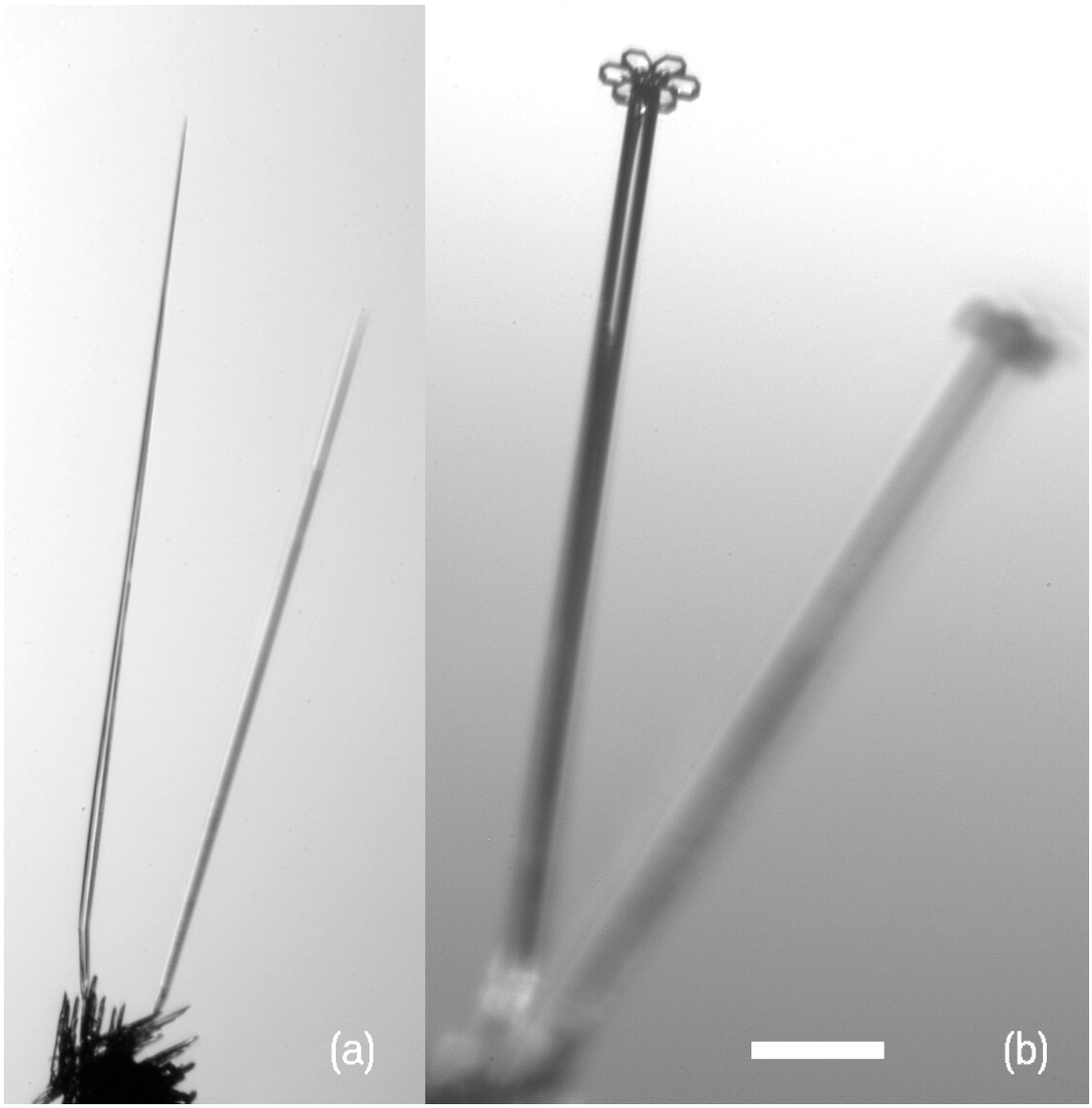

Figure 3. (a) Typical electric needle growth along the crystal c-axis at -5 C, which was induced using chemical additives (see text). (b) Subsequent growth at -15 C, after removing the applied electrical potential. Plates growing on the needle ends indicate the crystal orientation. The scale bar is 300 microns long.

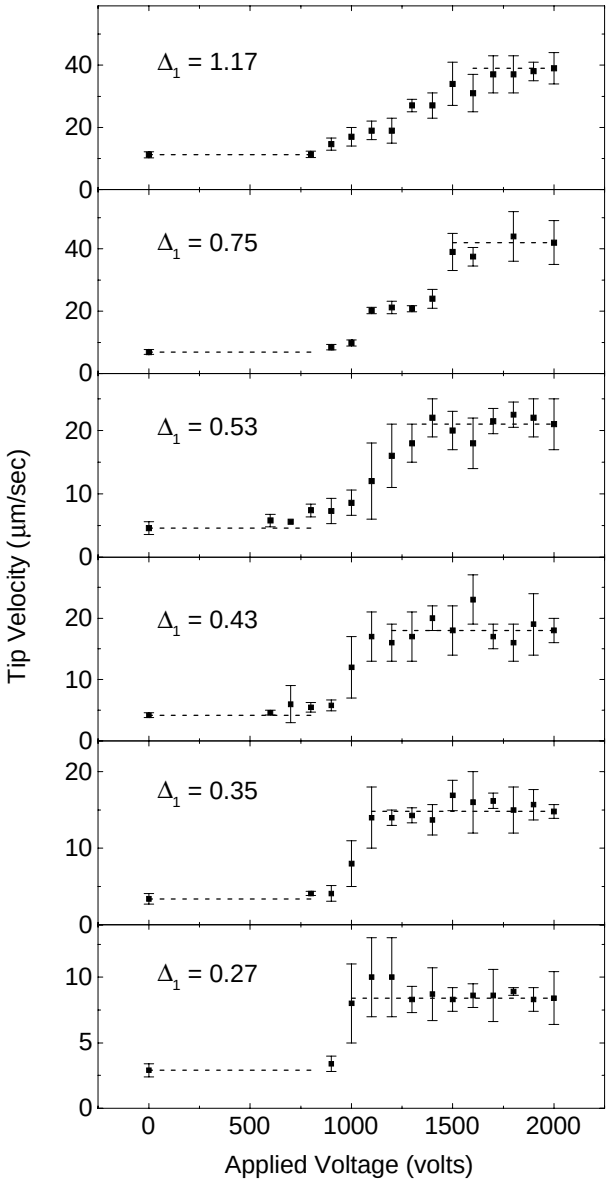

Figure 4. Tip velocities as a function of applied potential and supersaturation Δ_1, for ice needles grown at $T = -5$ C. Horizontal dotted lines were drawn through the first and last data points to guide the eye.

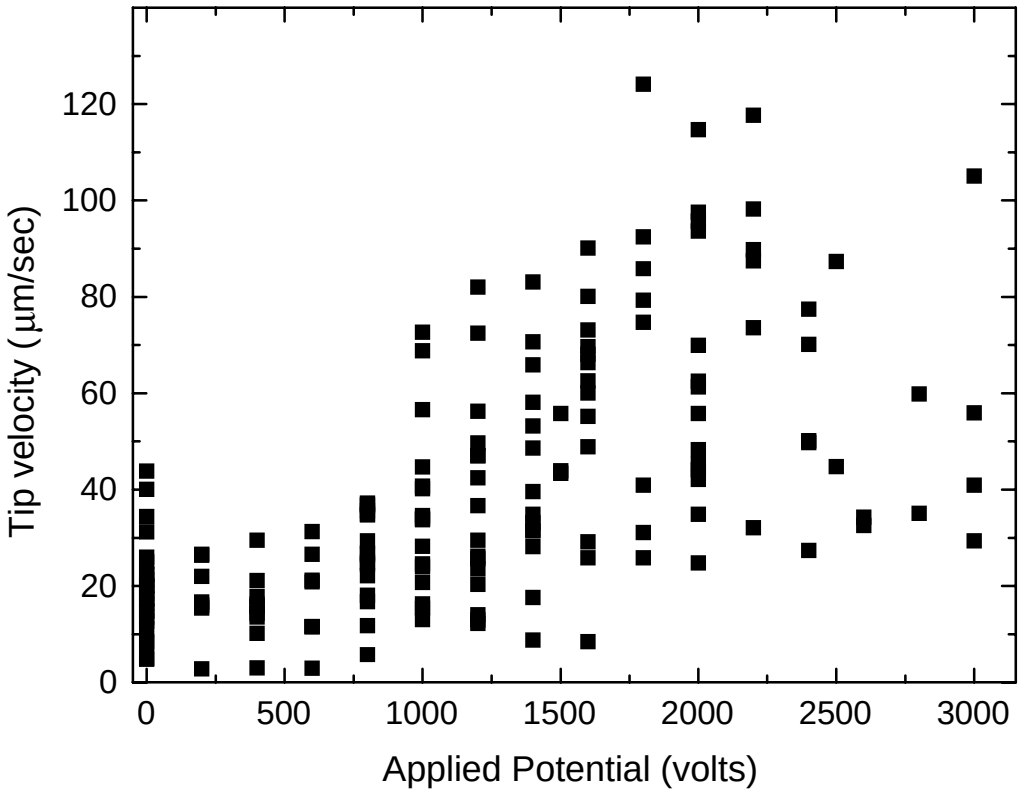

Figure 5. Tip velocities of growing iodine needle crystals as a function of the applied electrical potential. Each point represents the measurement of a single needle. Although the data show considerable scatter, there is clearly a large velocity increase above a threshold of ∼1000 volts, verifying the existence of this morphological instability for non-polar molecular systems.